Noname manuscript No.
(will be inserted by the editor)

Nonlinear Tubular Organ Modeling and Analysis for Tracheal Angioedema by Swelling-Morphoelasticity

Kun Gou · Pak-Wing Fok · Yibin Fu

Received: date / Accepted: date

Abstract We study one of the important human tubular organs, the trachea, under deformation caused by the disease angioedema. This pathology can suddenly increase the volume of the trachea and cause serious breathing difficulty. Two popular theories, the swelling theory and morphoelasticity theory, which generalize classical hyperelasticity to study material deformation under internal volume change, are integrated into a single model to study tracheal angioedema. Computational modeling results from various combinations of swelling and morphoelasticity are compared to exhibit the difference and similarity of the two theories in modeling tracheal angioedema. Nonlinear behaviors of the tubular radius change are also illustrated to show how the trachea luminal size alteration depends on the swelling/growth parameters and their effect on modifying tissue stiffness. The possibility of complete tracheal channel closure is also studied to understand if it is possible for the angioedema to close the airway. This article serves as an exemplary study on nonlinear deformation behaviors of human tubular organs with multiple layers.

Keywords Trachea · Angioedema · Swelling · Morphoelasticity · Hyperelasticity · Growth

K. Gou
Texas A&M University-San Antonio, Department of Science and Mathematics, San Antonio, Texas 78224, USA. E-mail: kun.gou@tamusa.edu

P.-W. Fok
Department of Mathematical Sciences, University of Delaware, Newark, Delaware 19716, USA. E-mail: pakwing@udel.edu

Y. Fu
School of Computing and Mathematics, Keele University, Staffordshire, ST5 5BG, UK. E-mail: y.fu@keele.ac.uk

1 Introduction

The human body incorporates numerous tubular organs (TOs) responsible for transporting fluids, nutrients and waste products throughout the body. Typical TOs include blood vessels, lymphatic vessels, the colon, trachea and esophagus etc. They are mainly composed of soft tissues, and commonly exhibit nonlinear behaviors in size change [1,31], morphology [2,3], stress distribution [4] etc. This article uses the trachea under angioedema as an example to illustrate such behaviors. In particular, we model trachea angioedema (TA) using generalized hyperelasticity to see how size change and stress distribution demonstrate nonintuitive nonlinear behaviors.

The trachea is a TO adjacent to the esophagus. It provides a duct for air flow between the ambient environment and the two lungs. Structurally similar to many other TOs, it has multi-layers, and two distinct layers have been observed in it [5]. The inner layer consists of mucous/submucous soft tissue. A longitudinal fiber family is also shown in this layer [9]. The outer layer includes numerous incomplete C-shaped hyaline cartilage rings stacking one over another, with the mouth of the C-rings residing behind the esophagus [5].

TA refers to a disease under which the inner layer of the trachea accumulates fluid from blood vessel leakage through the difference of hydrostatic and osmotic pressures [10,21,22] and increases its volume rapidly [12]. Such volume increment is also accompanied by mass addition such as vasoactive mediators or histamine to the tracheal tissue [11]. This disease is mainly categorized into two types [11]: acquired angioedema and hereditary angioedema. The first kind is caused by a deficiency of acquired c1-inhibitor c1-INH, and the second one is an autosomal dominantly inherited blood disorder [14]. Regardless of types, a rapid occurrence of volume increment on the airway soft tissue may quickly narrow the opening passage for normal breathing and induce an unexpected emergency [15,16,17]. The pathophysiological principle of TA has been studied via lab experiments [11] or mathematical simulations[18, 19]. The volume increment of the trachea is a complicated process. Some researchers applied mass conservation [23], transport theory [6], fluid mechanics [7] etc. to model such process. However, these methods are inadequate for more accurately describing the luminal area change and stress distribution from a nonlinear continuum mechanics perspective, which are key factors for evaluation of how TA may generate breathing difficulty and damage the internal tissue.

Soft tissues exhibit behaviors such as anisotropy, nonhomogeneity, strain-rate dependence [20]. When subject to physiological loads, soft tissues can be approximated as elastic materials and are broadly modeled by hyperelasticity [13]. Presently, two popular theories are employed to model hyperelastic material under volume increment. The first one is the *swelling theory* (see e.g., [36, 37,38,39]). This theory generalizes the classical hyperelasticity to incorporate the swelling effect with a localized swelling parameter. After a free swelling for an originally stress-free isotropic material body without any constraint, the body remains stress free. The strain energy density function is accordingly

modified to reflect this effect. The second hyperelastic theory called *morphoelasticity* [26] also bears the capability of modeling material volume change, and is widely applied in modeling growth of biological tissues [40,41,42,43]. The total deformation gradient tensor is decomposed to include a product of an elastic tensor and a growth tensor. The elastic tensor is employed as the deformation gradient in the strain energy function to generate stress distribution, and its determinant is identical to one when the material is modeled by incompressibility. All the volume change caused by growth is prescribed in the growth tensor. Unlike the swelling theory, the strain energy density function is not modified in any extent. Via the growth tensor, the morphoelasticity theory is also capable of modeling anisotropic volume change.

In [24,29], Gou and Pence modeled TA employing the swelling theory. In [24], the trachea is idealized as a closed two-layered cylinder. The top and bottom ends are taken to be force-free[i], and the inner and outer boundary are taken to be traction-free. Such boundary conditions assume that the deformation is completely caused by internal swelling instead of any external constraint. Angioedema generates residual stress over the tracheal body, and demonstrates high stress concentration near the interface of the inner and outer layers. In another article [29], more realistic tracheal geometries are considered that include the back-side trachealis muscle and two bronchi. Stress distribution from all levels of modeling are very similar, which justifies that idealized modeling and more realistic modeling may mutually complement each other to allow a deeper understanding of TA.

In this article, the swelling theory and morphoelasticity theory are integrated into a single model. The combined *swelling-morphoelasticity* model contains swelling and morphoelasticity as special cases, and thus is more flexible in accommodating volumetric changes arising from different combinations of swelling and growth. We can also use the integrated treatment to understand the difference and similarity of tissue deformation under the two theories. For convenience of analysis and comparison, we idealize the trachea as a two-layered cylindrical tube following [24]. For TA, another issue deserving great attention is whether the angioedema-incurred expansion of the trachea can close the internal channel to completely prevent air flow. By intuition, large expansion may finally shrink the opening until it is totally closed. However, problems from nonlinear continuum mechanics can often be counter-intuitive.

The structure of the article is as follows. In Section 2, we briefly introduce the generalized hyperelasticity for both swelling and morphoelasticity. We also construct the integrated swelling-morphoelasticity model and analyze its properties. In Sec. 3, we set up models for TA, which occurs in the inner submucous layer of the two-layered cylindrical geometry. The computational results are demonstrated in Sec. 4, where we compare modeling results from several parameter sets showing different swelling and growth combinations. In Sec.5, we illustrate the non-monotonic change of the luminal radius

[i] Force free boundary conditions are different from traction-free boundary conditions. The force-free boundary condition means the integration of traction over the related boundary is annihilated.

with respect to the volume increment of the trachea, and rigorously analyze the conditions required for complete closure of the lumen under the swelling-morphoelasticity model. Then finally a summary discussion is given in Sec. 6 about the nonlinear TO behaviors of the trachea under angioedema.

2 Preliminaries

The undeformed and deformed configurations are denoted by Ω_0 and Ω, respectively. Let $\mathbf{X}$ be any generic point in Ω_0, and it is mapped to another point $\mathbf{x}$ in Ω via a mapping $\mathbf{x} = \chi(\mathbf{X})$. The deformation gradient tensor is given by $\mathbf{F} = \partial\chi(\mathbf{X})/\partial\mathbf{X}$. The right Cauchy-Green deformation tensor is then

$$\mathbf{C} = \mathbf{F}^{\mathrm{T}}\mathbf{F}, \tag{2.1}$$

with the principal invariants

$$I_1 = \mathrm{tr}\mathbf{C}, \quad I_2 = I_3\mathrm{tr}(\mathbf{C}^{-1}), \quad I_3 = \det\mathbf{C}. \tag{2.2}$$

Under any strain energy function W, the Cauchy stress tensor $\mathbf{T}$ is derived via

$$\mathbf{T} = -p\mathbf{I} + 2\mathbf{F}\frac{\partial W}{\partial \mathbf{C}}\mathbf{F}^{\mathrm{T}}, \tag{2.3}$$

where p is a constraint parameter and $\mathbf{I}$ is the identity tensor. $\mathbf{T}$ satisfies the equilibrium equation

$$\mathrm{div}\mathbf{T} = \mathbf{0}, \tag{2.4}$$

in the deformed configuration.

Soft tissues are usually light, so we ignore the body forces from gravity and other effects. Below we briefly review theories of swelling and morphoelasticity and form an integrated model based on them.

2.1 Swelling theory

The swelling theory is mainly applied to study fluid-filled expansion of a body. It is mainly employed in areas like gel expansion and soft tissue edema [8,29]. The local swelling parameter ν depicts the ratio of the local volume in Ω_0 and Ω. For inhomogeneous swelling, ν depends on the position vector $\mathbf{X}$. In this article, for simplicity we take ν to be homogeneous and thus a constant throughout the material body. Via the deformation gradient, one has

$$\det\mathbf{F} = \nu. \tag{2.5}$$

The right Cauchy-Green deformation tensor is defined by (2.1), and its invariants are given by (2.2). This theory can be applied in the context of both

incompressibility and compressibility. In the first case, we also call it *volume-specified* swelling theory. With $\nu \equiv 1$, we recover the classical incompressible hyperelastic theory[ii].

Under a natural free swelling for an isotropic material body, i.e. boundaries of the body are traction free and no residual stress is generated after the deformation, there is no elastic energy stored inside the body, and then $\mathbf{F} = \nu^{1/3}\mathbf{I}$. The energy function is generalized to reflect this result. We use the neo-Hookean model as an example to show how such generalization is performed. The neo-Hookean model is originally given by

$$W = \frac{\mu}{2}(I_1 - 3), \tag{2.6}$$

where μ is the shear modulus of the material. To incorporate swelling, it is generalized to

$$W = \frac{1}{2}\mu\nu^{q-2/3}(I_1 - 3\nu^{2/3}), \tag{2.7}$$

where q is a parameter to show how swelling impacts on stiffness of the material, and the defaulted value $q = 2/3$ means the swelling keeps stiffness unchanged. Other strain energy models can be generalized in a similar way to incorporate swelling.

Under a natural free swelling, the material body is stress free. The generalized relation between the Cauchy stress tensor $\mathbf{T}$ and the energy function W for the volume-specified modeling is [28]

$$\mathbf{T} = -p\mathbf{I} + \frac{2}{\nu}\mathbf{F}\frac{\partial W}{\partial \mathbf{C}}\mathbf{F}^{\mathrm{T}}. \tag{2.8}$$

2.2 Morphoelasticity

Morphoelasticity mainly studies growth of a body through mass addition to change its volume. The growth process causes stress redistribution inside the body, and such stress and growth also demonstrate a complicated inter-connected relationship. Continuum mechanics plays a fundamental role in studying growth and its stress effect. Rodriguez et al. [25] proposed that the deformation of a body is caused by both the growth and elastic response, and they decomposed the deformation gradient $\mathbf{F}$ into two parts. One part is the growth tensor showing how mass is added into the body, and the other one is the elastic tensor, a natural response to the external mechanical stimuli and the growth to keep the body in an equilibrium state. More specifically,

$$\mathbf{F} = \mathbf{F}_e\mathbf{F}_g, \tag{2.9}$$

[ii] The main features of swelling theory are in (2.5) and (2.8). We call it volume-specified theory to avoid confusion with the incompressible theory. Also notice that (2.5) is always satisfied in the analysis, different from compressible theory in the fact that det$\mathbf{F}$ can change after computation.

where $\mathbf{F}_e$ is the elastic tensor and $\mathbf{F}_g$ is the growth tensor. The right Cauchy-Green deformation tensor is defined to be on $\mathbf{F}_e$ only, i.e.,

$$\mathbf{C}_e = \mathbf{F}_e^{\mathrm{T}}\mathbf{F}_e. \tag{2.10}$$

One can also define the three invariants I_1^e, I_2^e and I_3^e of $\mathbf{C}_e$ according to (2.2).

All the volume change is incorporated in the growth tensor. The material is taken to be incompressible after growth, and then

$$\det\mathbf{F}_e = 1. \tag{2.11}$$

The Cauchy stress is only caused by the elastic deformation part. The classical strain energy functions need not to be updated, but the invariants used in the energy functions are from $\mathbf{C}_e$ now. Particularly, the neo-Hookean model becomes

$$W = \frac{\mu}{2}(I_1^e - 3). \tag{2.12}$$

Under any strain energy function W, the Cauchy stress tensor is derived as

$$\mathbf{T} = -p\mathbf{I} + 2\mathbf{F}_e\frac{\partial W}{\partial \mathbf{C}_e}\mathbf{F}_e^{\mathrm{T}}. \tag{2.13}$$

If $\mathbf{F}_g = \varepsilon\mathbf{I}$, where ε is a growth parameter, the growth is isotropic. Otherwise, we call it *anisotropic growth*. Partial or planar isotropic growth can also be defined. Under the cylindrical coordinate system with three coordinates (r, θ, z), if the growth over the radial and angular directions are identical, we call it r-θ isotropic growth. Similarly, we can have θ-z or r-z isotropic growth.

2.3 Swelling-morphoelasticity

Swelling and morphoelasticity can also be incorporated into a single model. The deformation includes both the growth part $\mathbf{F}_g$ and elastic part $\mathbf{F}_e$ as in (2.9). In this integrated model, however, the volume change contribution is from both the growth and elastic parts. The growth part is for the volume change caused purely from growth, while the elastic part is responsible for the volume change caused by swelling satisfying

$$\det\mathbf{F}_e = \nu. \tag{2.14}$$

A deformation cartoon is shown in Fig. 1 to show such structure. The Cauchy-Green tensor is identical to that defined in (2.10). The corresponding strain energy function is modified to include swelling represented by (2.14). When the neo-Hookean model is used, the updated one is

$$W = \frac{1}{2}\mu\nu^{q-2/3}(I_1^e - 3\nu^{2/3}). \tag{2.15}$$

The Cauchy stress tensor is derived via

$$\mathbf{T} = -p\mathbf{I} + \frac{2}{\nu}\mathbf{F}_e\frac{\partial W}{\partial \mathbf{C}_e}\mathbf{F}_e^{\mathrm{T}}. \tag{2.16}$$

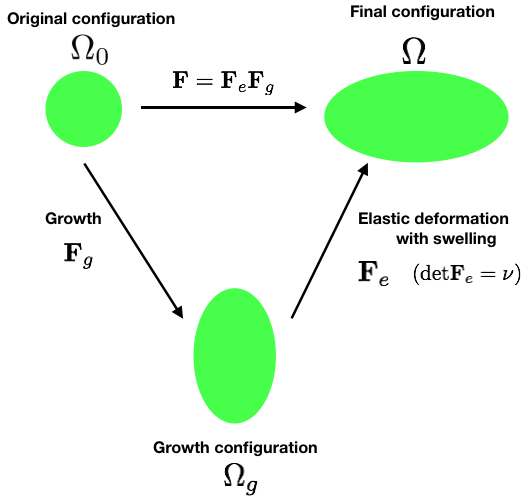

Fig. 1: Deformation cartoon for swelling-morphoelasticity. The original configuration is Ω_0. Then after growth with the growth tensor $\mathbf{F}_g$, we get a visual growth configuration Ω_g. An elastic deformation $\mathbf{F}_e$ is imposed on Ω_g to generate the final configuration Ω. Swelling is also incorporated in this step, and $\det\mathbf{F}_e = \nu$. The deformation gradient $\mathbf{F}$ from Ω_0 to Ω satisfies $\mathbf{F} = \mathbf{F}_e\mathbf{F}_g$.

We call such integration the *swelling-morphoelasticity* model. This treatment can easily reduce to either pure swelling hyperelastic theory via $\mathbf{F}_g = \mathbf{I}$ or morphoelasticity via $\nu = 1$.

3 TA modeling via swelling-morphoelasticity

The trachea is idealized to be a two-layered cylinder (Fig. 2). We work in a cylindrical coordinate system with the $z-$axis being the longitudinal direction of the trachea and the origin being the center of any of its horizontal cross section. The radii of the undeformed inner boundary, interface and outer boundary towards the central axis are denoted by R_i, R_m and R_o, respectively. Denote the three unit basis vectors of this coordinate system by $\mathbf{e}_R$, $\mathbf{e}_\Theta$ and $\mathbf{e}_Z$ for the undeformed configuration. Any point $\mathbf{X}$ in the undeformed configuration is denoted by (R, Θ, Z). We take the same set of basis vectors for the deformed configuration due to axisymmetry of the geometry and deformation. The point $\mathbf{X}$ is mapped into another point $\mathbf{x}$ on the deformed configuration via an axisymmetric deformation function χ

$$\mathbf{x} = \chi(\mathbf{X}) = r(R)\mathbf{e}_R + Z\lambda_z\mathbf{e}_Z, \tag{3.1}$$

where $r(R)$ is the radial function and λ_z is the axial stretch parameter. The radii of the deformed inner boundary, interface and outer boundary are $r_i = r(R_i)$, $r_m = r(R_m)$ and $r_o = r(R_o)$, respectively. The deformation gradient

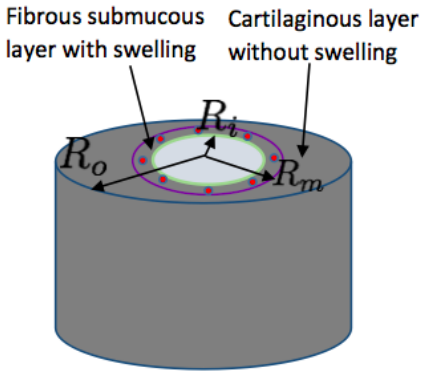

Fig. 2: An idealized two-layered trachea geometry. The inner thin layer is for submucous tissue where angioedema occurs. The red dots represent the vertically aligned collagen fibers in this layer in support of the stability of the tracheal structure. The outer thicker layer is the cartilaginous layer. This layer is mainly composed of a stack of harder cartilage rings and does not supply angioedema occurrence.

tensor is thus

$$\mathbf{F} = r'(R)\mathbf{e}_R \otimes \mathbf{e}_R + \frac{r}{R}\mathbf{e}_\Theta \otimes \mathbf{e}_\Theta + \lambda_z \mathbf{e}_Z \otimes \mathbf{e}_Z, \tag{3.2}$$

where the prime means differentiation.

3.1 Inner layer

The growth tensor is taken to be in the three principal directions as

$$\mathbf{F}_g = g_r \mathbf{e}_R \otimes \mathbf{e}_R + g_\theta \mathbf{e}_\Theta \otimes \mathbf{e}_\Theta + g_z \mathbf{e}_Z \otimes \mathbf{e}_Z, \tag{3.3}$$

where g_r, g_θ and g_z are growth parameters in the three principal directions, respectively.

By (2.9), (2.14) and (3.2)

$$\mathbf{F}_e = \frac{1}{\alpha}\mathbf{e}_R \otimes \mathbf{e}_R + \frac{\nu g_z}{\lambda_z}\alpha \mathbf{e}_\Theta \otimes \mathbf{e}_\Theta + \frac{\lambda_z}{g_z}\mathbf{e}_Z \otimes \mathbf{e}_Z, \tag{3.4}$$

where,

$$\alpha = \frac{g_r}{r'}, \qquad \frac{\nu g_z}{\lambda_z} g_\theta \alpha = \frac{r}{R}. \tag{3.5}$$

It then follows from (2.14) that

$$(r^2)' = \frac{2\nu g_r g_\theta g_z R}{\lambda_z}, \tag{3.6}$$

and so

$$r = \left[\int_{R_i}^{R} \frac{2\nu g_r g_\theta g_z R}{\lambda_z} \mathrm{d}R + r_i^2\right]^{1/2}, \quad R_i \le R \le R_m. \tag{3.7}$$

The parameters such as ν and g_r may be functions of R instead of constants, and thus (3.7) cannot be further simplified at this step. By (3.7), we can also derive the relation between r_m and r_i

$$r_m^2 = r_i^2 + \int_{R_i}^{R_m} \frac{2\nu g_r g_\theta g_z R}{\lambda_z} \mathrm{d}R, \tag{3.8}$$

which further generates another identical formula to (3.7)

$$r = \left[r_m^2 - \int_R^{R_m} \frac{2\nu g_r g_\theta g_z R}{\lambda_z} \mathrm{d}R \right]^{1/2}, \quad R_i \le R \le R_m. \tag{3.9}$$

The strain energy density function of the inner layer is taken to be the addition of the generalized neo-Hookean strain energy and longitudinal fiber energy as

$$W_i = \underbrace{\frac{\mu_i \nu^{q-2/3}}{2}(I_1^e - 3\nu^{2/3})}_{\text{neo-Hookean energy}} + \underbrace{\frac{\gamma}{2}(I_4^e - 1)^2}_{\text{fiber energy}}, \tag{3.10}$$

where μ_i is the shear modulus of the inner submucous layer, and γ is the fiber elastic modulus. In (3.10), I_4^e is defined as a pseudo-invariant as

$$I_4^e = \mathbf{N}_{fib} \cdot \mathbf{C}_e \mathbf{N}_{fib}, \tag{3.11}$$

where $\mathbf{N}_{fib} = \mathbf{e}_Z$ is the unit direction of the longitudinal fibers embedded in the submucous layer of the trachea. By (2.16), the Cauchy stress tensor is

$$\mathbf{T}^i = -p_i \mathbf{I} + \mu_i \nu^{q-5/3} \mathbf{B}_e + \frac{2\gamma}{\nu}(I_4^e - 1)\mathbf{E}_e \mathbf{e}_Z \otimes \mathbf{E}_e \mathbf{e}_Z, \tag{3.12}$$

where $\mathbf{B}_e = \mathbf{F_e F_e}^{\mathrm{T}}$ is a left Cauchy-Green tensor, and p_i is a constraint parameter dependent on R. Detailed computation gives the Cauchy stress in its component-wise form to be

$$T_{rr}^i = -p_i + \frac{\mu_i \nu^{q-5/3}}{\alpha^2}, \quad R_i \le R \le R_m, \tag{3.13}$$

$$T_{\theta\theta}^i = -p_i + \frac{\mu_i g_z^2 \nu^{q+1/3} \alpha^2}{\lambda_z^2}, \quad R_i \le R \le R_m, \tag{3.14}$$

$$T_{zz}^i = -p_i + \frac{\mu_i \lambda_z^2 \nu^{q-5/3}}{g_z^2} + \frac{2\gamma \lambda_z^2}{\nu g_z^2}\left(\frac{\lambda_z^2}{g_z^2} - 1\right), \quad R_i \le R \le R_m. \tag{3.15}$$

The three equilibrium equations in (2.4) for this axisymmetric model reduces to only one equation in the radial direction

$$\frac{\partial T_{rr}^i}{\partial r} + \frac{1}{r}(T_{rr}^i - T_{\theta\theta}^i) = 0. \tag{3.16}$$

By (3.13), (3.14) and (3.16), one has

$$p_i(R) = p_i(R_i)+ \\ \mu_i \int_{R_i}^{R} \nu^{q-5/3}\Big(\frac{(q-5/3)\nu^{-1}}{\alpha^2}\frac{\mathrm{d}\nu}{\mathrm{d}R} - 2\alpha^{-3}\frac{\mathrm{d}\alpha}{\mathrm{d}R} + \frac{1}{r}(\frac{1}{\alpha^2} - \frac{g_z^2\nu^2\alpha^2}{\lambda_z^2})\frac{\mathrm{d}r}{\mathrm{d}R}\Big)\mathrm{d}R. \tag{3.17}$$

3.2 Outer layer

There is no growth or swelling in the outer cartilaginous layer. Thus $\mathbf{F}_g = \mathbf{I}$ and $\nu = 1$. By the incompressibility constraint $\det\mathbf{F} = 1$, via (3.2)

$$\frac{r' r \lambda_z}{R} = 1. \tag{3.18}$$

Integration of (3.18) from R to R_o gives

$$r = \sqrt{r_o^2 - \frac{1}{\lambda_z}(R_o^2 - R^2)}, \quad R_m \le R \le R_o. \tag{3.19}$$

By (3.19), we can obtain the relation between r_m and r_o as

$$r_m^2 = r_o^2 - \frac{1}{\lambda_z}(R_o^2 - R_m^2), \tag{3.20}$$

which gives another formula for r as

$$r = \sqrt{r_m^2 + \frac{1}{\lambda_z}(R^2 - R_m^2)}, \quad R_m \le R \le R_o. \tag{3.21}$$

The strain energy density function is taken to be the original neo-Hookean model

$$W_o = \frac{\mu_o}{2}(I_1 - 3), \tag{3.22}$$

where μ_o is the shear modulus of the outer cartilaginous layer. The Cauchy stress tensor $\mathbf{T}^o$ for this layer is derived via W_o as

$$\mathbf{T}^o = -p_o\mathbf{I} + 2\mathbf{F}\frac{\partial W_o}{\partial \mathbf{C}}\mathbf{F}^{\mathrm{T}} = -p_o\mathbf{I} + \mu_o\mathbf{B}, \tag{3.23}$$

where $\mathbf{B} = \mathbf{F}\mathbf{F}^{\mathrm{T}}$ is the left Cauchy-Green tensor for the outer layer, and p_o is a constraint parameter for this layer. Detailed computation gives the Cauchy stress in its component-wise form to be

$$T_{rr}^o = -p_o + \mu_o(r')^2, \quad R_m \le R \le R_o, \tag{3.24}$$

$$T_{\theta\theta}^o = -p_o + \mu_o r^2/R^2, \quad R_m \le R \le R_o, \tag{3.25}$$

$$T_{zz}^o = -p_o + \mu_o\lambda_z^2, \quad R_m \le R \le R_o. \tag{3.26}$$

As in (3.16), we get one equilibrium equation in the radial direction

$$\frac{\partial T^o_{rr}}{\partial r} + \frac{1}{r}(T^o_{rr} - T^o_{\theta\theta}) = 0. \tag{3.27}$$

By virtue of (3.24), (3.25) and (3.27), we get

$$p_o(R) = p_o(R_o) - \mu_o \int_R^{R_o} r'\Big(2r'' + r^{-1}\big((r')^2 - \frac{r^2}{R^2}\big)\Big)\mathrm{d}R. \tag{3.28}$$

3.3 Boundary conditions and solution procedure

The inner boundary of the tracheal tube is subject to aerial flow to and from the two lungs. The pressure is close to the atmospheric pressure which can be balanced by the pressure inside the tracheal tissue. We thus ignore the effect on the inner boundary of the trachea exerted by the air flow inside the lumen, and take the inner boundary of the trachea tube to be traction free. The outer boundary of the trachea tube is surrounded by light soft tissue, and taken to be traction free as well. The traction-free inner and outer boundary conditions are given by

$$\begin{cases} T^i_{rr}(r_i) = 0 \quad \text{(traction-free inner boundary)}, \\ T^o_{rr}(r_o) = 0 \quad \text{(traction-free outer boundary)}. \end{cases} \tag{3.29}$$

By (3.13) and $(3.29)_1$, we get

$$p_i(R_i) = \frac{\mu_i \nu^{q-5/3}}{\alpha^2}\Big|_{R=R_i}, \tag{3.30}$$

and by (3.24) and $(3.29)_2$, we have

$$p_o(R_o) = \mu_o (r')^2|_{R=R_o}. \tag{3.31}$$

At the interface, the traction is taken to be continuous, which gives

$$T^i_{rr}(r_m) = T^o_{rr}(r_m) \quad \text{(traction continuous at the interface)}, \tag{3.32}$$

or by (3.13) and (3.24)

$$-\,p_i(R_m) + \frac{\mu_i \nu^{q-5/3}}{\alpha^2}\Big|_{R=R_m} = -p_o(R_m) + \mu_o (r')^2\big|_{R=R_m}. \tag{3.33}$$

The radial function $r(R)$ is also continuous throughout the interface in the domain $[R_i, R_o]$ automatically by our formulation. Namely, $r(R)$ in (3.9) for the inner submucous layer and $r(R)$ in (3.21) for the outer cartilaginous layer are equal when both estimated at $R = R_m$. Using (3.9) and (3.21), (3.33) is an equation for the unknown r_m. This nonlinear equation can be solved by numerical techniques. With the value of r_m, we can obtain the Cauchy stress distribution $\mathbf{T}$ and radial function $r(R)$ for the two layers.

Radius values (unit:mm)				
	Notation	Inner boundary	Interface	Outer boundary
Original size:	R	R_i=8.85	R_m=9.15	R_o=11.45
After deformation:	r	r_i	r_m	r_o

Table 1: Radius values before and after deformation caused by angioedema. The radius values before deformation for the inner boundary, interface and outer boundary are taken from [24,29]. The corresponding boundary radii after deformation are unknowns and their values are calculated from the present model.

Tracheal stiffness parameters (unit: MPa)		
Inner layer shear modulus	Outer layer shear modulus	Fiber stiffness
μ_i=0.0429	μ_o=0.58	γ=0.0429

Table 2: Tracheal tissue stiffness values used in the model. These value are kept to be identical to those used in [24,29] for consistency.

4 Modeling results and comparison

The radius values for R_i, R_m and R_o are taken from [24,29] as shown in Table 1. The material stiffness values are illustrated in Table 2 [iii]. We use the defaulted value $q = 2/3$ for the computation in this section, i.e., the volume increment shall not change the stiffness of the tissue. The product of all growth and swelling parameters ν, g_r, g_θ and g_z is fixed for convenience of comparison. This makes the total volume change under the collective effect of growth and swelling of the submucous layer after TA identical. The product

$$\nu g_r g_\theta g_z = 4, \tag{4.1}$$

is used, where the number 4 is randomly chosen for a clearer view and comparison of the solutions. This large parameter is for the purpose of mathematical study only. More realistic parameters for volume change of the trachea under angioedema can be found in references, e.g. [45], where they found a more conservative parameter around 1.2. As to the authors' best knowledge, no literature has been found to make any experimental or clinic study on the proportions of swelling and growth in TA. Because the swelling theory is for volume change in 3-D, first we consider 3-D isotropic growth in the swelling-morphoelasticity model and then 2-D isotropic growth.

4.1 3-D isotropic growth

Isotropic growth means growth in the three principal directions $\mathbf{e}_R$, $\mathbf{e}_\Theta$ and $\mathbf{e}_Z$ are identical, i.e., $g_1 = g_2 = g_3 = g$, where g is a constant. Then we have

[iii] These values were calculated from experimental data via justified mathematical formulas. See [24].

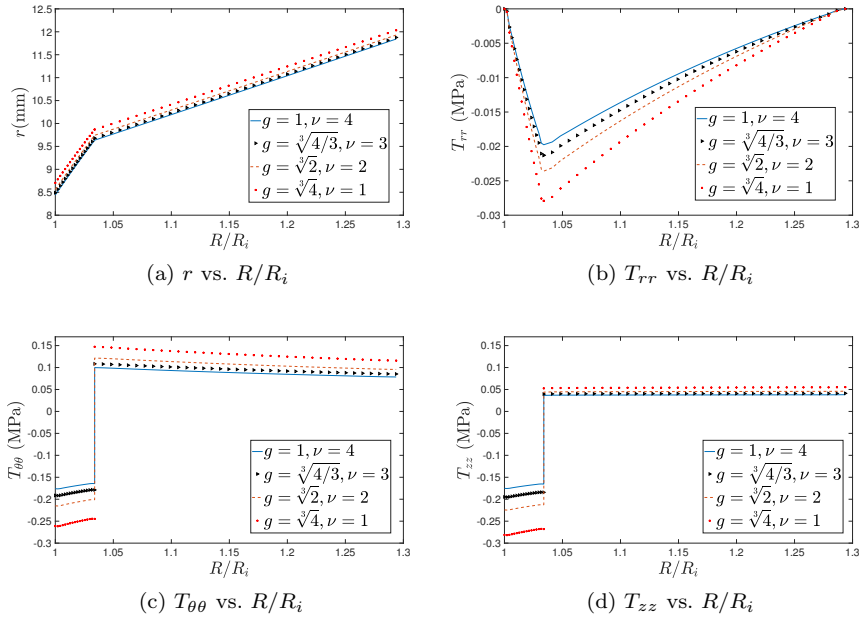

(a) r vs. R/R_i (b) T_{rr} vs. R/R_i

(c) $T_{\theta\theta}$ vs. R/R_i (d) T_{zz} vs. R/R_i

Fig. 3: Radius change and stress distribution as functions of R for various combinations of swelling and 3-D isotropic growth parameters ν, g_r, g_θ, and g_z satisfying $g_r = g_\theta = g_z = g$. Here R is normalized by R_i. The product of all growth and swelling parameters is kept to be a constant 4, i.e., $g^3\nu = 4$. There is no stretch in the axial direction ($\lambda_z = 1$), and the defaulted value $q = 2/3$ is used. The plots illustrate that increased g or decreased ν generates increased r_i (decreased trachea opening constriction) and increased stress magnitude at each fixed R.

$g^3\nu = 4$ by (4.1). We use four sets of parameters as a demonstration:

$$S_1 : \{g = 1, \nu = 4\}, \quad S_2 : \{g = \sqrt[3]{4/3}, \nu = 3\},$$
$$S_3 : \{g = \sqrt[3]{2}, \nu = 2\}, \quad S_4 : \{g = \sqrt[3]{4}, \nu = 1\}.$$

Set S_1 shows only swelling without growth ($g = 1$), and Set S_4 shows only growth without swelling ($\nu = 1$). They are the two extreme ends of the swelling-morphoelasticity modeling. The other two sets are mix of both swelling and growth.

Figure 3 illustrates the results under an axial stretch $\lambda_z = 1$. First we give a summary for the general patterns of all curves. Due to the volume increment of the inner submucous layer from TA, Figure 3a shows that the inner radius r_i is reduced and the outer radius r_o is increased for the parameter set choice. We also remark that in this panel the curves over the inner layer or outer layer are almost straight, but they are nonlinear curves. Figure 3b shows that the radial stress T_{rr} is compressive, and reaches its maximum at the interface, which

makes the tissue more vulnerable at this location. The curves also show cusps indicating non-smoothness at the interface because only traction continuity condition is prescribed at this location. Figures 3c and 3d for $T_{\theta\theta}$ and T_{zz} vs. R, respectively, show compressive stress in the inner layer, tensile stress in the outer layer, and stress discontinuities at the interface. According to Fig. 3, over the range for R from R_i to R_o the variation for T_{rr} is much smaller than $T_{\theta\theta}$ and T_{zz}.

Then we compare the curves in each subfigure for the four sets $S1$-$S4$. Figure 3a shows that Set S_1 for pure swelling gives the lowest r vs. R curve, while Set S_4 gives the highest, or more generally, more growth or less swelling makes the curve higher. Therefore, under the same volume change, modeling TA using more swelling produces more inner opening shrinkage. In Figures 3b-3d, at a fixed R location, Set S_1 generates the smallest stress magnitude and Set S_4 generates the largest, or more generally, more growth generates larger stress magnitude. One possible explanation for this phenomenon is that more growth makes the trachea expand more outward, and thus the inner submucous layer pushes the outer cartilaginous layer more outward resulting in bigger stress production. More growth hence may more seriously hurt the tracheal tissue bearing stronger stress.

Computation for $\lambda_z = 1.3$ is also taken. For each set of parameters, the inner opening is more constrained, and smaller stress intensity is produced. However, the results show no different pattern compared with Fig. 3, and the graph is thus skipped.

4.2 2-D isotropic growth

We study how the results will differ when the isotropic growth is constrained in 2-D. Three types are studied: isotropic r-θ growth, isotropic r-z growth, and isotropic θ-z growth.

4.2.1 Isotropic r-θ growth

We consider planar isotropic growth over the radial and angular directions. Here we take $g_r = g_\theta$ and $g_z = 1$ satisfying $g_r^2\nu = 4$ according to (4.1). $\lambda_z = 1$ is also used. Four sets of parameters are used:

$$S_5 : \{g_r = g_\theta = 1, g_z = 1, \nu = 4\}, \quad S_6 : \{g_r = g_\theta = 2\sqrt{1/3}, g_z = 1, \nu = 3\},$$
$$S_7 : \{g_r = g_\theta = \sqrt{2}, g_z = 1, \nu = 2\}, \quad S_8 : \{g_r = g_\theta = 2, g_z = 1, \nu = 1\}.$$

The general pattern of the results for these four parameter sets shown in Fig. 4 are similar to that in Fig. 3. For all four sets, Fig. 4 demonstrates identical curves for $r(R)$, $T_{rr}(R)$ or $T_{\theta\theta}(R)$. For the axial stress T_{zz}, all four curves are the same over the outer cartilaginous layer and disagree over the inner submucous layer (Set S_8 for pure growth with $\nu = 1$ generates the least T_{zz} intensity over the inner layer). Therefore, in the swelling-morphoelasticity model,

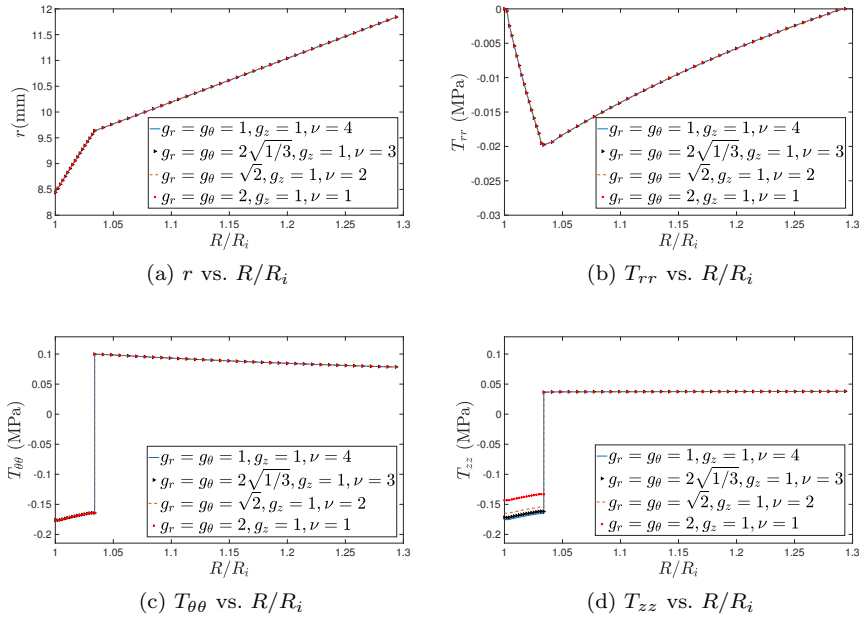

(a) r vs. R/R_i (b) T_{rr} vs. R/R_i

(c) $T_{\theta\theta}$ vs. R/R_i (d) T_{zz} vs. R/R_i

Fig. 4: Radius change and stress distribution of various combinations of swelling and 2-D isotropic growth ($g_r = g_\theta, g_z = 1$), where the growth is constrained to be on the radial and angular directions. The product of all growth and swelling parameters is kept to be a constant 4, i.e., $g_r g_\theta g_z \nu = 4$. Here $\lambda_z = 1$ and $q = 2/3$. The graphs show that the four sets generate the same results for radius change and T_{rr} and $T_{\theta\theta}$ distributions, and T_{zz} is identical only in the outer layer.

computational results are identical regardless of how swelling and growth are mixed. Nonzero T_{zz} values also suggest that planar r-θ growth is not completely constrained in the r-θ plane, and also generates stress in the axial direction outside of the r-θ plane.

In order to test how different axial stretch can affect the deformation, we also used $\lambda_z = 1.3$ in the computation for the four sets $S5$-$S8$. The same pattern is maintained as in Fig. 4, and hence the graphs are not displayed here for the sake of brevity. It is also found that larger λ_z may generate all tensile stress over the two layers for T_{rr} and $T_{\theta\theta}$ instead of being compressive over the inner layer and tensile over the outer layer for smaller λ_z. Larger λ_z also produces smaller r_i giving more constrained inner opening and causing more difficulty for breathing.

4.2.2 Isotropic r-z and θ-z growth

The computational results of isotropic r-z or θ-z growth do not show a nice overlap for different combinations of swelling and growth as those for isotropic

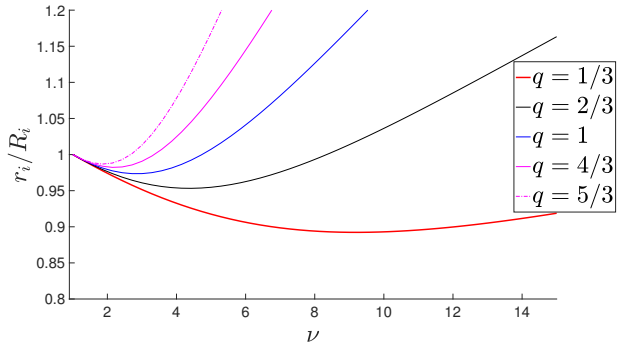

Fig. 5: Graph of how r_i(normalized by R_i) changes based on total volume increment for various q values indicating how volume increment alters stiffness of the material. The label for the horizontal axis "volume increment ratio" (vir) means the pointwise volume ratio after and before angioedema satisfying $vir = \det\mathbf{F} = \det\mathbf{F}_e \det\mathbf{F}_g$. Isotropic r-θ growth is used in the swelling-morphoelasticity model with growth parameters satisfying $g_z = 1$ and $g_r = g_\theta$. For each value of vir, the contributions from swelling (with the swelling parameter ν) and total growth are the same, i.e., $\nu = \sqrt{vir}$ and $g_r g_\theta = \sqrt{vir}$. Each curve is non-monotonic. The function $r_i(vir)$ decreases and then increases.

r-θ growth. Generally the plots are similar to Fig. 3 and therefore not shown here for the sake of brevity.

5 Luminal shrinkage

When the trachea is under angioedema, the volume of the inner layer expands. Quantitative and qualitative understanding of the expansion is necessary for accurate description of severity of the disease. Based on the model setup in Sec. 3, we graphically obtain relations between inner radius change and volume increment amount. Then we study when it is possible for the angioedema to totally close the luminal area to obstruct air flow.

5.1 Dependence of r_i on volume increment

The idealized modeling for the tracheal geometry allows us to quantify the luminal area in terms of the deformed inner radius r_i. We study the relation between r_i and the volume increment from both swelling and growth so that we can know how luminal area changes. From Sec. 4, we see that the swelling-morphoelasticity model with r-θ isotropic growth shows almost identical modeling results regardless of how much volume change contribution is from swelling or growth as far as the total volume change is fixed. Such 2-D r-θ isotropic growth also closely matches the axisymmetric deformation formulation in (3.1). We also use such isotropic growth in this section for convenience of analysis. Figure 5 shows several curves of r_i (normalized by R_i) vs. volume

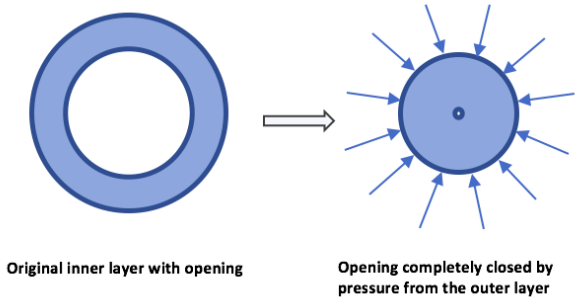

Fig. 6: Anticavitation cartoon for the inner submucous layer with completely closed luminal area under pressure from the outer cartilaginous layer.

increment ratio for several q values indicating how volume change alters the shear modulus of the tissue. For each curve, it shows the inner radius first decreases and then increases. This implies that the lumen does not always shrink but can also expand when r_i reaches a minimum value. Larger q makes the minimum value larger.

5.2 Further anticavitation analysis

We analyze if it is possible for the outer cartilaginous layer to push the inner submucous layer using only finite force such that the inner opening is completely collapsed under TA, which we call *anticavitation* (Fig. 6). Similar problems have been examined by other researchers. Abeyaratne and Hou studied void collapse for an incompressible spherical elastic solid [33], and Moulton and Goriely studied anticavitation and differential growth in elastic shells by morphoelasticity [34]. The present work takes swelling and growth together to study the possibility of tubular collapse. For this purpose, we only consider the deformation of the inner layer, and the effect of the outer layer is to impose a traction on the inner layer. Denote the traction imposed by the outer layer through the interface to the inner layer by

$$-P_{\rm tr} = T^i_{rr}|_{R=R_m}, \tag{5.1}$$

where $P_{\rm tr} > 0$.

For any strain energy function W (not only the neo-Hookean model), consider it depends on the three principal stretches Λ_r, Λ_θ and Λ_z associated with the elastic tensor $\mathbf{F}_e$ as $W(\Lambda_r, \Lambda_\theta, \Lambda_z)$. We remark that usually an energy function is considered to depend on the invariants I_1, I_2 and I_3 etc., and such stretch dependence of the energy function is solely for convenience of the present analysis. Under the swelling-morphoelasticity model in Sec. 2.3 and the axisymmetric deformation in (3.1)

$$\mathbf{F}_e = \Lambda_r \mathbf{e}_R \otimes \mathbf{e}_R + \Lambda_\theta \mathbf{e}_\Theta \otimes \mathbf{e}_\Theta + \Lambda_z \mathbf{e}_Z \otimes \mathbf{e}_Z, \tag{5.2}$$

and by virtue of (3.4),

$$\Lambda_r = \frac{1}{\alpha}, \quad \Lambda_\theta = \frac{\nu g_z \alpha}{\lambda_z}, \quad \Lambda_z = \frac{\lambda_z}{g_z}. \tag{5.3}$$

By (2.14),

$$\Lambda_r = \frac{\nu g_z}{\lambda_z \Lambda_\theta}, \quad \frac{\mathrm{d}\Lambda_r}{\mathrm{d}\Lambda_\theta} = -\frac{g_z \nu}{\lambda_z \Lambda_\theta^2}. \tag{5.4}$$

We consider P_{tr} as a function of Λ_θ, and analyze under what condition

$$\lim_{\Lambda_\theta^i \to 0} P_{\mathrm{tr}} < \infty,$$

where $\Lambda_\theta^i = \Lambda_\theta|_{r=r_i}$.

Generalizing the function W to include swelling with the swelling parameter ν for the inner layer generates

$$W_i = \nu^q W(\nu^{-1/3}\Lambda_r, \nu^{-1/3}\Lambda_\theta, \nu^{-1/3}\Lambda_z). \tag{5.5}$$

Notice that if W is of the neo-Hookean model incorporating the fiber energy, then (5.5) gives (3.10), the generalized neo-Hookean model. Under (2.16),

$$T_{rr}^i = -p_i + \frac{2}{\nu}\Lambda_r^2 \frac{\partial W_i}{\partial C_{rr}^e} = -p_i + \frac{\Lambda_r}{\nu}\frac{\partial W_i}{\partial \Lambda_r}, \tag{5.6}$$

$$T_{\theta\theta}^i = -p_i + \frac{2}{\nu}\Lambda_\theta^2 \frac{\partial W_i}{\partial C_{\theta\theta}^e} = -p_i + \frac{\Lambda_\theta}{\nu}\frac{\partial W_i}{\partial \Lambda_\theta}, \tag{5.7}$$

where C_{rr}^e and $C_{\theta\theta}^e$ are the first two principal components of $\mathbf{C_e}$.

It is convenient to use $(5.4)_1$ to eliminate Λ_r from the right hand side of (5.5) and define the resulting expression as $\hat{W}_i(\Lambda_\theta)$, where dependence of the reduced energy function $\hat{W}_i$ on Λ_z is not shown explicitly for the sake of brevity since Λ_z is always assumed to be fixed in our calculations. It can then easily be shown that

$$T_{rr}^i - T_{\theta\theta}^i = -\frac{\Lambda_\theta}{\nu}\frac{\mathrm{d}\hat{W}_i}{\mathrm{d}\Lambda_\theta}, \tag{5.8}$$

and so the equilibrium equation (3.16) can be written as,

$$\frac{\mathrm{d}T_{rr}^i}{\mathrm{d}r} = \frac{\Lambda_\theta}{r\nu}\frac{\mathrm{d}\hat{W}_i}{\mathrm{d}\Lambda_\theta}. \tag{5.9}$$

Integrating (5.9) with respect to r from r_i to r_m produces

$$\int_{r_i}^{r_m} \frac{\mathrm{d}T_{rr}^i}{\mathrm{d}r}\mathrm{d}r = \frac{1}{\nu}\int_{r_i}^{r_m} \frac{\Lambda_\theta}{r}\frac{\mathrm{d}\hat{W}_i}{\mathrm{d}\Lambda_\theta}\mathrm{d}r. \tag{5.10}$$

Traction free inner boundary $T_{rr}^i|_{r=r_i} = 0$ and (5.1)applied to (5.10) give

$$P_{\mathrm{tr}} = -\frac{1}{\nu}\int_{r_i}^{r_m} \frac{\Lambda_\theta}{r}\frac{\mathrm{d}\hat{W}_i}{\mathrm{d}\Lambda_\theta}\mathrm{d}r = -\frac{1}{\nu}\int_{\Lambda_\theta^i}^{\Lambda_\theta^m} \Lambda_\theta \frac{\mathrm{d}\hat{W}_i}{\mathrm{d}\Lambda_\theta}\frac{\mathrm{d}(\ln r)}{\mathrm{d}\Lambda_\theta}\mathrm{d}\Lambda_\theta. \tag{5.11}$$

By (3.7) with constant ν, g_r, g_θ, g_z and λ_z, we get

$$r = \Big(\frac{\nu g_r g_\theta g_z}{\lambda_z}(R^2 - R_i^2) + r_i^2\Big)^{1/2} \quad \text{or} \quad R = \Big(\frac{\lambda_z(r^2 - r_i^2)}{\nu g_r g_\theta g_z} + R_i^2\Big)^{1/2}. \tag{5.12}$$

Then by $(3.5)_2$, $(5.3)_2$ and (5.12),

$$\Lambda_\theta = \frac{r}{g_\theta R} = r g_\theta^{-1}\Big(\frac{\lambda_z(r^2 - r_i^2)}{\nu g_r g_\theta g_z} + R_i^2\Big)^{-1/2}. \tag{5.13}$$

Solving for r from (5.13) generates

$$r = \Lambda_\theta\Big(\frac{g_\theta(\lambda_z r_i^2 - R_i^2 \nu g_r g_\theta g_z)}{\Lambda_\theta^2 g_\theta \lambda_z - \nu g_r g_z}\Big)^{1/2}. \tag{5.14}$$

By (5.14),

$$\frac{\mathrm{d}(\ln r)}{\mathrm{d}\Lambda_\theta} = \frac{-\nu g_r g_z}{\Lambda_\theta\big(\Lambda_\theta\sqrt{g_\theta\lambda_z} + \sqrt{\nu g_r g_z}\big)\big(\Lambda_\theta\sqrt{g_\theta\lambda_z} - \sqrt{\nu g_r g_z}\big)}. \tag{5.15}$$

Plugging (5.15) into (5.11) brings

$$P_{\mathrm{tr}} = \int_{\Lambda_\theta^i}^{\Lambda_\theta^m} \frac{\mathrm{d}\hat{W}_i}{\mathrm{d}\Lambda_\theta} \frac{g_r g_z}{\big(\Lambda_\theta\sqrt{g_\theta\lambda_z} + \sqrt{\nu g_r g_z}\big)\big(\Lambda_\theta\sqrt{g_\theta\lambda_z} - \sqrt{\nu g_r g_z}\big)} \mathrm{d}\Lambda_\theta. \tag{5.16}$$

Lemma 1 *For an r-θ isotropic (isotropy over the r-θ plane) one-layered TO under swelling (with the swelling parameter ν) and isotropic growth (with three principal growth parameters g_r, g_θ and g_z satisfying $g_r = g_\theta$), the following inequality holds*

$$\frac{d\hat{W}_i}{d\Lambda_\theta}\big(\Lambda_\theta\sqrt{g_\theta\lambda_z} - \sqrt{\nu g_r g_z}\big) > 0. \tag{5.17}$$

Proof For a planar r-θ isotropic material under r-θ isotropic growth and swelling, the Baker-Ericksen inequality [35] holds due to the strong ellipticity:

$$(T_{rr}^i - T_{\theta\theta}^i)(\lambda_r - \lambda_\theta) > 0, \tag{5.18}$$

where λ_r and λ_θ are two principal stretches associated with $\mathbf{F}$ in the r and θ directions, respectively, satisfying $\lambda_r = \Lambda_r g_r$ and $\lambda_\theta = \Lambda_\theta g_\theta$. By the definition of Λ_r and Λ_θ in (5.3) and Eq. (3.4), one has $\alpha = \frac{\Lambda_\theta \lambda_z}{\nu g_z}$. Accordingly,

$$\begin{aligned}\lambda_r - \lambda_\theta &= \frac{g_r}{\alpha} - \frac{\nu g_z \alpha g_\theta}{\lambda_z} \\ &= \frac{\big(\sqrt{g_r g_z \nu} - \Lambda_\theta\sqrt{g_\theta\lambda_z}\big)\big(\sqrt{g_r g_z \nu} + \Lambda_\theta\sqrt{g_\theta\lambda_z}\big)}{\Lambda_\theta\lambda_z}.\end{aligned} \tag{5.19}$$

By (5.8) for $T_{rr}^i - T_{\theta\theta}^i$ and Eq. (5.19), one thus obtains (5.17) for the lemma.

Lemma 2 *For $\Lambda_\theta^i \le \Lambda_\theta \le \Lambda_\theta^m$, we have $\Lambda_\theta\sqrt{g_\theta\lambda_z} - \sqrt{\nu g_r g_z} < 0$ as r_i approaches 0 and is sufficiently small.*

Proof By $(5.3)_2$ and $(3.5)_1$,

$$\begin{aligned}\Lambda_\theta\sqrt{g_\theta\lambda_z}-\sqrt{\nu g_r g_z}&=\sqrt{g_\theta\lambda_z}\frac{\nu g_z}{\lambda_z}\alpha-\sqrt{\nu g_r g_z}\\&=\sqrt{g_\theta\lambda_z}\frac{\nu g_z}{\lambda_z}g_r(\frac{\mathrm{d}r}{\mathrm{d}R})^{-1}-\sqrt{\nu g_r g_z}\\&=\frac{\sqrt{\lambda_z}r}{\sqrt{g_\theta}R}-\sqrt{\nu g_r g_z}.\end{aligned}\tag{5.20}$$

By the volume relation between the reference configuration and the deformed configuration,

$$(R_m^2-R_i^2)\nu g_r g_\theta g_z=(r_m^2-r_i^2)\lambda_z,\tag{5.21}$$

we can obtain

$$r_m=\sqrt{\frac{(R_m^2-R_i^2)\nu g_r g_\theta g_z}{\lambda_z}+r_i^2}.\tag{5.22}$$

By (5.20) and (5.22),

$$\lim_{r_i\to 0}(\Lambda_\theta\sqrt{g_\theta\lambda_z}-\sqrt{\nu g_r g_z})\Big|_{r=r_m}=\sqrt{\nu g_r g_z}\Big(\sqrt{1-\frac{R_i^2}{R_m^2}}-1\Big)<0.\tag{5.23}$$

Therefore, as $r_i\to 0$ and is sufficiently small, we have $\Lambda_\theta\sqrt{g_\theta\lambda_z}-\sqrt{\nu g_r g_z}<0$ for all $\Lambda_\theta^i\le\Lambda_\theta\le\Lambda_\theta^m$.

By Lemmas 1 and 2 applied to (5.16), one has

$$\begin{aligned}0<P_{\mathrm{tr}}&<\sqrt{\frac{g_r g_z}{\nu}}\int_{\Lambda_\theta^i}^{\Lambda_\theta^m}\frac{\mathrm{d}\hat{W}_i}{\mathrm{d}\Lambda_\theta}\frac{\mathrm{d}\Lambda_\theta}{\Lambda_\theta\sqrt{g_\theta\lambda_z}-\sqrt{\nu g_r g_z}}\\&<\sqrt{\frac{g_r g_z}{\nu}}\frac{1}{\Lambda_\theta^m\sqrt{g_\theta\lambda_z}-\sqrt{\nu g_r g_z}}\int_{\Lambda_\theta^i}^{\Lambda_\theta^m}\frac{\mathrm{d}\hat{W}_i}{\mathrm{d}\Lambda_\theta}\mathrm{d}\Lambda_\theta\\&=\sqrt{\frac{g_r g_z}{\nu}}\frac{1}{\Lambda_\theta^m\sqrt{g_\theta\lambda_z}-\sqrt{\nu g_r g_z}}\Big(\hat{W}_i|_{\Lambda_\theta=\Lambda_\theta^m}-\hat{W}_i|_{\Lambda_\theta=\Lambda_\theta^i}\Big)\\&=K\Big(\hat{W}_i|_{\Lambda_\theta=\Lambda_\theta^i}-\hat{W}_i|_{\Lambda_\theta=\Lambda_\theta^m}\Big),\end{aligned}\tag{5.24}$$

where $K=\sqrt{\frac{g_r g_z}{\nu}}\frac{1}{\sqrt{\nu g_r g_z}-\Lambda_\theta^m\sqrt{g_\theta\lambda_z}}>0$.

Theorem 3 *The inner submucous layer can be completely collapsed under finite pressure from the outer cartilaginous layer if and only if the following is true*

$$\lim_{\Lambda_\theta^i\to 0}\hat{W}_i|_{\Lambda_\theta=\Lambda_\theta^i}=\mathbb{L}<\infty,\tag{5.25}$$

where $\mathbb{L}$ *is any positive finite number.*

Proof If (5.25) holds, then by (5.24), $P_{\rm tr}|_{\Lambda_\theta^i=0}$ is bounded, and finite pressure is possible to totally collapse the lumen of the trachea.

Instead, if $P_{\rm tr}|_{\Lambda_\theta^i=0}$ is bounded, we show (5.25) is true. By Lemma 2,

$$0 > -\frac{1}{\sqrt{\nu g_r g_z}} > \frac{1}{\Lambda_\theta\sqrt{g_\theta\lambda_z} - \sqrt{\nu g_r g_z}}, \tag{5.26}$$

for $\Lambda_\theta^i \le \Lambda_\theta \le \Lambda_\theta^m$. Thus by (5.16)

$$\begin{aligned} P_{\rm tr} &> -\frac{1}{\sqrt{\nu g_r g_z}}\int_{\Lambda_\theta^i}^{\Lambda_\theta^m}\frac{{\rm d}\hat{W}_i}{{\rm d}\Lambda_\theta}\frac{g_r g_z}{\big(\Lambda_\theta\sqrt{g_\theta\lambda_z}+\sqrt{\nu g_r g_z}\big)}{\rm d}\Lambda_\theta \\ &> \frac{-\sqrt{g_r g_z}}{\sqrt{\nu}\big(\Lambda_\theta^m\sqrt{g_\theta\lambda_z}+\sqrt{\nu g_r g_z}\big)}\int_{\Lambda_\theta^i}^{\Lambda_\theta^m}\frac{{\rm d}\hat{W}_i}{{\rm d}\Lambda_\theta}{\rm d}\Lambda_\theta \\ &= \frac{\sqrt{g_r g_z}}{\sqrt{\nu}\big(\Lambda_\theta^m\sqrt{g_\theta\lambda_z}+\sqrt{\nu g_r g_z}\big)}\big(\hat{W}_i|_{\Lambda_\theta=\Lambda_\theta^i} - \hat{W}_i|_{\Lambda_\theta^m}\big), \end{aligned} \tag{5.27}$$

where we also used $\frac{{\rm d}\hat{W}_i}{{\rm d}\Lambda_\theta} < 0$ obtained from Lemmas 1 and 2. Since $\hat{W}_i$ as an energy function is always non-negative and $\lim\limits_{\Lambda_\theta^i\to 0} P_{\rm tr}$ is bounded, we get

$$\infty > \lim_{\Lambda_\theta^i\to 0}\hat{W}_i|_{\Lambda_\theta=\Lambda_\theta^i} \ge 0, \tag{5.28}$$

which gives (5.25).

Corollary 1 *For the generalized neo-Hookean model (2.7) incorporating swelling, the anticavitation of the inner submucous layer cannot occur under finite pressure from the outer cartilaginous layer.*

Proof By (5.2) and (5.3), $I_1 = {\rm tr}\mathbf{C}_e = \Lambda_r^2 + \Lambda_\theta^2 + \Lambda_z^2$ and $I_4 = \Lambda_z^2$ (fiber direction parallel to the $\mathbf{e}_z$ direction). And then (2.14) gives $\Lambda_r = \frac{\nu}{\Lambda_\theta\Lambda_z}$. The generalized neo-Hookean model (3.10) becomes

$$\hat{W}_i = \frac{\mu_i\nu^{q-2/3}}{2}\Big((\frac{\nu}{\Lambda_\theta\Lambda_z})^2 + \Lambda_\theta^2 + \Lambda_z^2 - 3\nu^{2/3}\Big) + \frac{\gamma}{2}(\Lambda_z^2-1)^2, \tag{5.29}$$

which easily shows that

$$\lim_{\Lambda_\theta^i\to 0}\hat{W}_i|_{\Lambda_\theta=\Lambda_\theta^i} = \infty. \tag{5.30}$$

Therefore, by Theorem 3, the present generalized neo-Hookean model is incapable of closing the inner channel through finite pressure imposed on the inner submucous layer by the outer cartilaginous layer.

For the neo-Hookean model coefficient $\frac{\mu_i\nu^{q-2/3}}{2}$ in (3.10), $\lim\limits_{q\to-\infty}\frac{\mu_i\nu^{q-2/3}}{2} = 0$ means that the updated shear modulus of the tissue is annihilated due to swelling, and thus

$$\lim_{\Lambda_\theta^i\to 0}(\hat{W}_i|_{q\to-\infty,\Lambda_\theta=\Lambda_\theta^i}) = 0.$$

So by Theorem 3 the total collapse is possible with finite pressure from the outer layer under this extreme case.

6 Summary and discussion

The trachea is one of the most important human tubular organs. When angioedema occurs in this organ, the normal size of the inner lumen may change, which can cause serious breathing difficulty. In this paper, the trachea is idealized as a two-layered cylinder. Angioedema is taken to occur in the inner softer layer, and the outer cartilaginous layer is modeled as being incompressible. Since we neglected air flow in the duct and the effect of supporting tissues around the trachea, the inner and outer boundaries of the tube are assumed to be traction free.

TA is modeled employing an integrated nonlinear swelling-morphoelasticity treatment. Both swelling and morphoelasticity generalize hyperelasticity to account for volume changes in a continuum body. However, they are designed from different perspectives. In swelling, the deformation gradient from the undeformed to the final deformed configuration is used in the updated strain energy function to derive the stress distribution, and the volume change is used to constrain the determinant of the deformation gradient tensor. In morphoelasticity, the deformation gradient is decomposed into the product of a growth tensor and an elastic tensor, but only the elastic tensor is employed to generate the stress distribution. Volume change is included through the growth tensor. The swelling-morphoelasticity treatment combines the two theories into a single model. It is more versatile for modeling deformations induced by volume changes, since the volume increment can be distributed between swelling *and* growth: the exact contributions from each component can be specified by the user or dictated by the pathophysiology of TA. For example, volume changes in TA could arise from swelling caused by fluid from leaky blood vessels and from solid growth caused by mass addition to the tracheal tissue [11]. The integrated treatment can also be employed in compressible models [27] for finite-element computational need. We also remark that a complete thermomechanics and constitutive relation analysis for the swelling-morphoelasticity model deserves study to build up a stronger theoretical foundation for it. A thorough analysis for this aspect is needed in future research.

Computational results are given for the deformed radius r vs. the undeformed radius R, and the three principal Cauchy stress components T_{rr}, $T_{\theta\theta}$, and T_{zz} vs. R. The graphs of T_{rr} vs. R show that residual stress concentrates near the interface of the two layers. Graphs for $T_{\theta\theta}$ vs. R and T_{zz} vs. R are discontinuous through the interface, indicating that the tissue is under compression in the inner layer and under tension in the outer layer. Theories of morphoelasticity and swelling are structurally different, but we found that the computational results for the swelling, morphoelasticity and their combinations are qualitatively similar to each other. Interestingly, we also found that, for a given volume change, any combination of swelling and 2-D r-θ isotropic morphoelastic growth gives almost identical results for the deformation and stress profiles, but different combinations of swelling and 3-D morphoelastic growth (again, for a fixed volume change) generally give different profiles. A summary of the computational results from Sec. 4 is given in Table 3. Fur-

	r	$\lvert T_{rr}\rvert$	$\lvert T_{\theta\theta}\rvert$	$\lvert T_{zz}\rvert$
3-D i.g.:	Growth dom.	Growth dom.	Growth dom.	Growth dom.
r-θ i.g.:	The same	The same	The same	The same over $[R_m, R_o]$
r-z i.g.:	Swelling dom.	Swelling dom.	Swelling dom.	Swelling dom.
θ-z i.g.:	Growth dom.	Growth dom.	Growth dom.	Growth dom.

Table 3: Summary of computational results comparison for the swelling-morphoelasticity model. The same amount of volume increment caused by a combination of swelling and growth is used for all the comparisons. Here "i.g." stands for isotropic growth, and "dom." is the abbreviation of "dominate". The symbol $\lvert\bullet\rvert$ means the absolute value of the quantity inside. For the row of 3-D isotropic growth, "Growth dom." means more growth and less swelling generate larger material radius change and magnitude of T_{rr}, $T_{\theta\theta}$, and T_{zz} under the same R location. So does the row for θ-z isotropic growth. For the r-z isotropic growth, the trend is the opposite. For the r-θ isotropic growth row, the results are always the same (except T_{zz}) regardless of how combination of swelling and growth contribution to the volume increment is made.

ther investigation is needed to understand why deformation and stress are so insensitive to different combinations of swelling and r-θ growth.

We also show that the inner radius is non-monotonic with respect to volume change. The deformed inner radius r_i decreases as the inner layer volume increases in the beginning, but after the volume increment reaches some threshold, r_i unexpectedly increases, generating a larger lumen. This nonlinear characteristic is also exhibited in other TOs. For example, Glagov et al. [32] experimentally found that coronary arteries with atherosclerotic plaques along the inner arterial wall initially increase their luminal area, but later as the stenosis increases, the luminal area decreases. Fok [30] employed morphoelasticity theory to model plaque growth and successfully captured this nonmonotonic trend. He also found that the monotonicity depended on whether vessels were pressurized or not. However, the behavior of r_i with respect to volume increment in the trachea is concave up, rather than concave down, which is due to mechnical and structural differences between arteries and tracheae.

To further explore the nonlinear inner radius change and check if complete lumen closure is possible, an anticavitation analysis is made based on general strain energy density functions for the swelling-morphoelasticity model. Realistically, anticavitation under effects such as irregular geometry, buckling behavior, air flow, and mucosal membrane adhesive should be considered in the analysis for more practical application. For the sake of brevity we skip these effects in this analysis. The theoretical analysis focuses on the inner layer, assuming the outer layer imposes an inward pressure on the boundary. We rigorously show that the lumen can be completely closed with finite force from the outer layer if and only if the strain energy remains finite as the angular stretch goes to zero. The commonly used neo-Hookean model does not satisfy this requirement. Therefore in our idealized model of angioedema, it is theoretically impossible to completely close off a trachea no matter how much growth or swelling occurs. The result in Theorem 3 is similar to the requirements for the collapse of an incompressible spherical elastic solid studied in [33,34] for materials modeled by classical hyperelasticity and morphoelasticity,

respectively. It indicates that the more generalized hyperelasticity model does not change the requirements for the collapse of a solid body with an internal void under limited pressure imposed on the outer boundary.

The present article is based on an idealized cylindrical geometry for which the inner surface is always smooth under axisymmetric deformation. In reality, when under volume increment from either growth or swelling, the inner wall of soft tissues may demonstrate an asymmetric buckling behavior [2,3,38,44]. One can study these instabilities for an axisymmetric base state, and finite element approaches can be employed for more general settings. Even in the axisymmetric setting, it would be interesting to see how the classical buckling analysis changes under the swelling-morphoelasticity model. As shown in [46] by Li et al, the angioedema pathology generally induces non-uniform volume increment along the circumferential direction, so further study should be performed to model this nonuniform volume change on TA applying swelling-morphoelasticity.

Although the present work focuses on a particular organ (the trachea), our results are indicative of multi-layer TOs modeled using hyperelasticity, and the framework in this paper can be used to understand TO deformation problems arising from other physiological conditions. Because different layers of the TO have different stiffness parameters, thicknesses and fiber properties, we expect deformations and stress distribution in general to be non-smooth and non-monotonic with respect to the radial coordinate. Stresses may concentrate near the interface between different layers, making the tissue there more vulnerable to damage or dislocation. Finally, we predict that in general, TOs will not close their lumens completely when their inner layers experience growth and/or swelling.

Acknowledgment Pak-Wing Fok is supported by a Simons Foundation collaboration grant #282579. Kun Gou is grateful to the 2018 Texas A&M University-San Antonio Research Council Grant and the College of Arts and Sciences Summer Faculty Research Fellowship.

References

1. Beitel GJ, Krasnow MA (2000) Genetic control of epithelial tube size in the Drosophila tracheal system. Dev 127:3271-3282
2. Ciarletta P, Balbi V, Kuhl E (2014) Pattern selection in growing tubular tissues. Phys Rev Lett 113:248101:1-5
3. Ciarletta P, Amar MB (2012) Pattern formation in fiber-reinforced tubular tissues: folding and segmentation during epithelial growth. J Mech Phys Solids 60(3):525-537
4. Gregersen H, Barlow J, Thompson D (1999) Development of a computer-controlled tensiometer for real-time measurements of tension in tubular organs. Neurogastroenterol 11:109-118
5. Minnich DJ, Mathisen DJ (2007) Anatomy of the trachea, carina, and bronchi. Thorac Surg Clin 17(4):571-585
6. Gu WY, Lai WM, Mow VC (1998) A mixture theory for charged-hydrated soft tissues containing multi-electrolytes: passive transport and swelling behaviors. J Biomech Eng 120(2):169-180

7. Singh PP, Cushman JH, Maier DE (2003) Multiscale fluid transport theory for swelling biopolymers. Chem Eng Sci 58(11):2409-2419
8. Baek S, Pence TJ (2011) Inhomogeneous deformation of elastomer gels in equilibrium under saturated and unsaturated conditions. J Mech Phys Solids 59:561-582
9. Wang L, Tepper R, Bert JL, Pinder KL, Par PD, Okazawa M (2000) Mechanical properties of the tracheal mucosal membrane in the rabbit. I. Steady-state stiffness as a function of age. J Appl Physiol 88:1014-1021
10. Katz MA, Bresler EH (1984) Osmosis. In: Edema, p 39-46
11. Temio VM, Peebles RS (2008) The spectrum and treatment of angioedema. Am J Med 121:282-286
12. Greaves M, Lawlor F (1991) Angioedema: manifestations and management. J Am Acad Dermatology 25:155-165
13. Natali AN, Carniel EL, Pavan PG, Dario P, Izzo I (2006) Hyperelastic models for the analysis of soft tissue mechanics: definition of constitutive parameters. In: The First IEEE/RAS-EMBS International Conference on Biomedical Robotics and Biomechatronics, p 1-8
14. Bork K (2006) Hereditary angioedema with normal c1 inhibitor activity including hereditary angioedema with coagulation factor xii gene mutations. Immunol Allergy Clin North Am 26:709-724
15. Krnacik MJ, Heggeness MH (1997) Severe angioedema causing airway obstruction after anterior cervical surgery. Spine 22:2188-2190
16. Ishoo E, Shah UK, Grillone GA, Stram JR, Fuleihan NS (1999) Predicting airway risk in angioedema: staging system based on presentation. Otolaryngol Head Neck 121:263-268
17. Bork K, Hardt J, Schicketanz KH, Ressel N (2003) Clinical studies of sudden upper airway obstruction in patients with hereditary angioedema due to C1 esterase inhibitor deficiency. Arch Intern Med 163:1229-1235
18. Brown RH, Zerhouni EA, Mitzner W (1995) Airway edema potentiates airway reactivity. J Appl Physiol 79:1242-1248
19. Amin SD, Majumdar A, Frey U, Suki B (2010) Modeling the dynamics of airway constriction: effects of agonist transport and binding. J Appl Physiol 109:553-563
20. Holzapfel GA (2001) Biomechanics of soft tissue. In: The handbook of materials behavior, p 1-12
21. Aukland K, Reed RK (1993) Interstitial-lymphatic mechanisms in the control of extracellular fluid volume. Physiol Rev 73:1-78
22. Reed RK (1979) An implantable colloid osmometer: Measurements in subcutis and skeletal muscle of rats. Microvasc Res 18:83-94
23. Bennethum LS, Cushman JH (1996) Multiscale, hybrid mixture theory for swelling systems-I: balance laws. Int J Eng Sci 34:125-145
24. Gou K, Pence TJ (2016) Hyperelastic modeling of swelling in fibrous soft tissue with application to tracheal angioedema. J Math Biol 72:499-526
25. Rodriguez EK, Hoger A, McCulloch AD (1994) Stress-dependent finite growth in soft elastic tissues. J Biomech 27:455-467
26. Goriely A, Moulton D (2011) Morphoelasticity: a theory of elastic growth. Oxford University Press
27. Pence TJ, Gou K (2015) On compressible versions of the incompressible neo-Hookean material. Math Mech Solids 20:157-182
28. Demirkoparana H, Pence TJ (2007) Swelling of an internally pressurized nonlinearly elastic tube with fiber reinforcing. Int J Solids Struct 44:4009-4029
29. Gou K, Pence TJ (2017) Computational modeling of tracheal angioedema due to swelling of the submucous tissue layer. Int J Numer Method Biomed Eng. DOI: 10.1002/cnm.2861
30. Fok PW (2016) Multi-Layer mechanical model of Glagov remodeling in coronary arteries: Differences between In-Vivo and Ex-Vivo Measurements. PloS one 11: e0159304
31. Fok PW, Sanft R (2015) A biochemical and mechanical model of injury-induced intimal thickening. Math Med Biol 34:77-108
32. Glagov S, Weisenberg E, Zarins CK, Stankunavicius R, Kolettis GJ (1987) Compensatory enlargement of human atherosclerotic coronary arteries. N Engl J Med 316:1371-1375

33. Abeyaratne R, Hou HS (1991) Void collapse in an elastic solid. J Elast 26:23-42
34. Moulton DE, Goriely A (2011) Anticavitation and differential growth in elastic shells. J Elast 102:117-132
35. Fosdick R, Silhavy M (2006) Generalized Baker-Ericksen inequalities. J Elast 85:39-44
36. Tsai H, Pence TJ (2004) Swelling induced finite strain flexure in a rectangular block of an isotropic elastic material. J Elast 75:69-89
37. Pence TJ, Tsai H (2006) Swelling-induced cavitation of elastic spheres. Math Mech Solids 11:527-551
38. Demirkoparan H (2017) Bulging bifurcation of inflated circular cylinders of doubly fiber-reinforced hyperelastic material under axial loading and swelling. Math Mech Solids 22(4):666-682
39. Demirkoparan H, Merodio J (2017) Swelling-twist interaction in fiber-reinforced hyperelastic materials: the example of azimuthal shear. J Eng Math. DOI 10.1007/s10665-017-9906-x
40. Goriely A, Moulton DE, Vandiver R (2010) Elastic cavitation, tube hollowing, and differential growth in plants and biological tissues. Europ Lett 91:18001:1-6
41. Balbi V, Ciarletta P (2013) Morpho-elasticity of intestinal villi. J R Soc Interface 10:20130109:1-12
42. Goriely A, Amar MB (2007) On the definition and modeling of incremental, cumulative, and continuous growth laws in morphoelasticity. Biomech Model Mechanobiol 6:289-296
43. Bowden LG, Byrne HM, Maini PK (2016) A morphoelastic model for dermal wound closure. Biomech Model Mechanobiol 15:663-681
44. Li B, Cao YP, Feng XQ, Gao H (2012) Mechanics of morphological instabilities and surface wrinkling in soft materials: a review. Soft Matter 8:5728-5745
45. Woie K, Reed RK (1996) The relationship between interstitial fluid pressure and volume in rat trachea. Acta Physiol Scand 156:6974
46. Li B, Cao Y-P, Feng X-Q, Gao H (2011) Surface wrinkling of mucosa induced by volumetric growth: Theory, simulation and experiment. J Mech Phys Solids 59:758-774